

## HYBRID BEARINGS FOR LH<sub>2</sub> AND LO<sub>2</sub> TURBOPUMPS

M. F. Butner and F. C. Lee

Rockwell International/Rocketdyne Division  
Canoga Park, California

### Abstract

Hybrid combinations of hydrostatic and ball bearings can improve bearing performance for liquid hydrogen and liquid oxygen turbopumps. Analytic studies were conducted to optimize hybrid bearing designs for the SSME-type turbopump conditions. A method to empirically determine damping coefficients was devised. Four hybrid bearing configurations were designed, and three were fabricated. Six hybrid and hydrostatic-only bearing configurations will be tested for steady-state and transient performance, and quantification of damping coefficients. The initial tests have been conducted with the liquid hydrogen bearing.

### Turbopump Bearing Improvement is Needed

In the Space Shuttle Main Engine (SSME) turbopumps, the use of propellant-cooled ball bearings achieves reduced turbopump size and weight by eliminating the need for separate lubricants, and the attendant seals and heaters. The SSME High Pressure Oxidizer Turbopump (HOPTP) represents this practice (Fig. 1). Ball bearings are capable of functioning in the severe environments typical of turbopumps, where high speeds and loads are combined with large temperature excursions, negligible lubrication and particulate contamination. Ball bearings with 440-C balls and races and Teflon-fiber-glass cages were entirely satisfactory for liquid hydrogen and liquid oxygen service in single-flight engines like the J-2 used in the Apollo Program.

With the advent of reusable vehicles, the SSME and other advanced engine requirements have placed progressively greater demands on turbopump bearings in terms of life, load capacity, speed capability, and rotor support

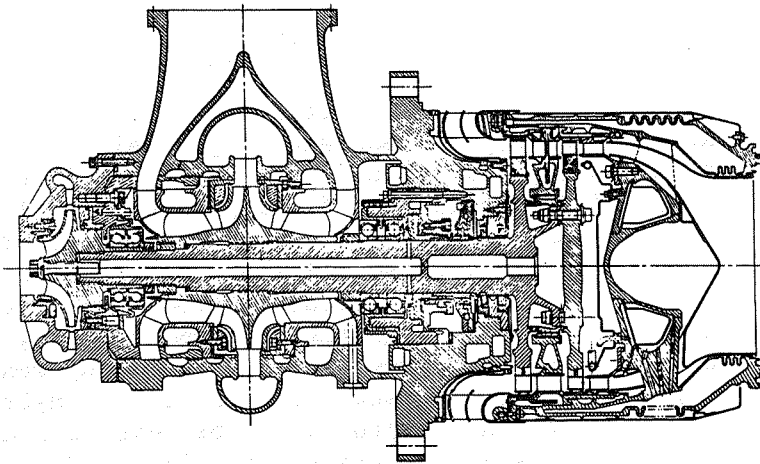


Fig. 1. SSME HPOTP Cross Section

characteristics, taxing the capabilities of ball bearings. For example, the SSME service life requirement of 7.5 hours exceeds the 1 to 3 hours bearing life currently attained under operating conditions like those listed in Table 1. Speed capabilities exceeding  $2 \times 10^6$  DN, with service lives of 10 hours are required for advanced applications in the near future with further increases anticipated. Ball bearings are currently limited to approximately  $2 \times 10^6$  DN by centrifugal loading and wear. Rotordynamic response could often be improved if increases in shaft diameter, bearing stiffness, and/or damping were available.

Table 1. SSME HPOTP Bearing Operating Conditions

	HPOTP		HPFTP
	PREBURNER	TURBINE END	
COOLANT	LO <sub>2</sub>	LO <sub>2</sub>	LH <sub>2</sub>
COOLANT TEMPERATURE, R	210	210	90
SPEED, RPM	30,000	30,000	36,000
BEARING DN, 10 <sup>6</sup>	1.4	1.7	1.6
LOAD (PER BEARING)			
AXIAL, TRANSIENT	SMALL	4,000	NEGLIGIBLE
AXIAL, STEADY STATE	850	1,000	700
RADIAL, FIXED	500	500	SMALL
RADIAL, SYNCHRONOUS	600	600	400 - 900

## Hybrid Bearings Can Fill Need

Hydrostatic bearings are attractive alternates to ball bearings, as they can operate at journal speeds up to approximately  $5 \times 10^6$  DN, show increased load capacity (providing sufficient fluid pressure and flow are available), and in addition can provide improved shaft support through greater stiffness and damping. However, since they require pressurization from an external source to develop significant load capacity, hydrostatic bearings need some means of avoiding wear and heat generation during start and shutdown. Hybrid combinations of ball and hydrostatic bearings such as shown in Fig. 2 possess dry start capability and can exploit the advantages of the film bearing. These bearings are adaptable to rocket turbomachinery, since typical liquid rocket flow systems can supply the high pressure fluid required for hydrostatic bearings without significant performance penalty. One or more of the possible hybrid bearing forms possess the characteristics necessary for achievement of life and performance goals for individual bearing positions in the SSME and future engine turbopumps. Hybrid bearings have been tested, demonstrated to be feasible, and are actively considered for incorporation into new designs (Ref. 1-3).

### Program to Develop Hybrid Bearing Technology

NASA/Lewis Research Center (LeRC) initiated the SSME Long Life Bearing Program under Contract NAS3-23263 with the goal of extending bearing capabilities by providing practical design information for radial hybrid bearings suitable for SSME and other advanced propulsion systems. The program comprises design studies, bearing fabrication, testing, and correlation of analytic and empirical results.

### Design Studies

#### Hybrid Bearing Designs

Hydrostatic and ball bearing elements can be combined to share speed or load; working fluid may be

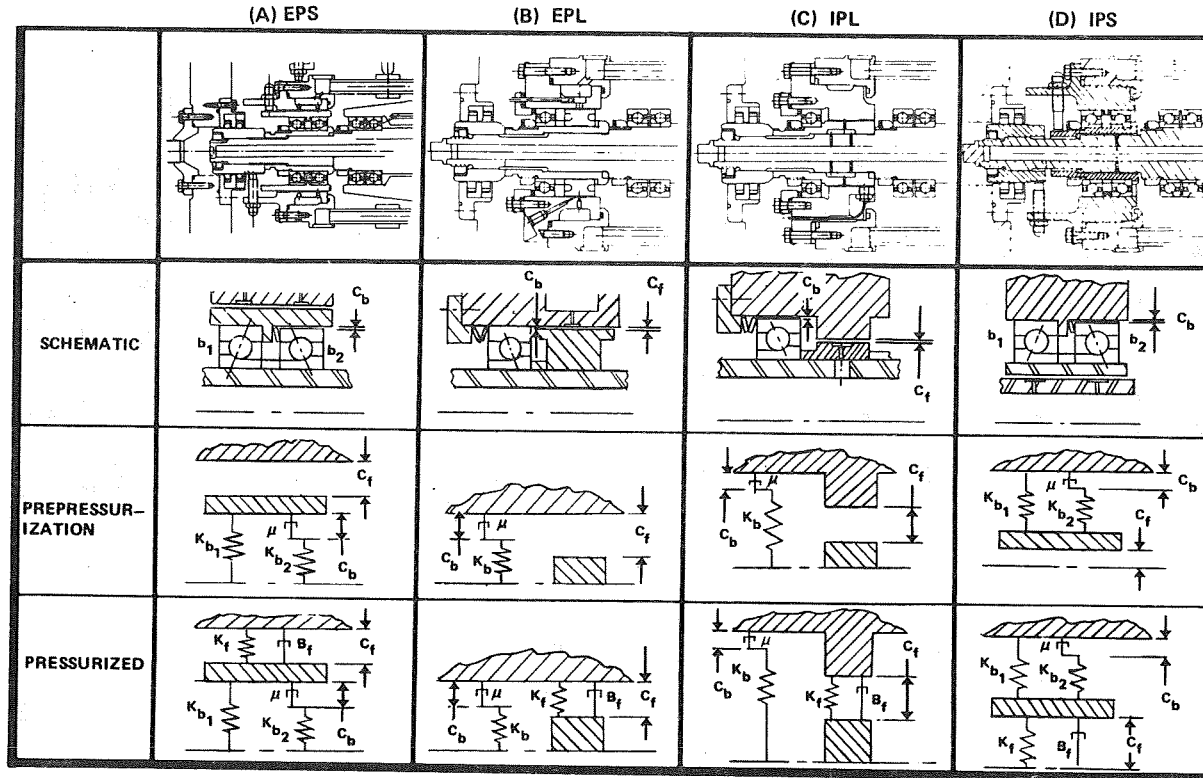


Fig. 2. Hybrid Bearing Types

supplied externally or from the shaft center. Figure 2 presents the four types of hybrid bearing most applicable to rocket engine turbopumps. The following abbreviations will be used to identify the several configurations in the balance of this paper:

1. EPS--Externally Pressurized, Parallel Speed
2. EPL--Externally Pressurized, Parallel Load
3. IPL--Internally Pressurized, Parallel Load
4. IPS--Internally Pressurized, Parallel Speed

In Fig. 2, the top row is a cross section of the design as installed in the test rig. The second row contains the bearing pictorial schematic. Functional schematics are shown prior to pressurization (Row 3) and fully pressurized (Row 4). Symbols for Fig. 2 are defined as:

- b - designates ball bearing (also used as subscript)
- f - designates film bearing (also used as subscript)
- c - radial clearance
- $\mu$  - Coulomb friction
- B - viscous damping
- K - stiffness

#### Bearing Analyses

Hybrid bearing performance was predicted by combining the characteristics of the hydrostatic and ball bearing members for conditions representing start, steady-state, and shutdown conditions based on SSME speeds and loads. Hydrostatic bearing analyses were performed using the computer program HBEAR written by Artilles, Wallwit, and Shapiro (Ref. 4). Stiffness, friction torque, and flow were determined as functions of speed and clearance for selected bearing geometry. The hydrostatic bearing analytical model assumes incompressible fluid and isothermal flow, in which the

turbulent effect on the fluid's viscosity and the inertia effect at the recess boundary are included. The last two effects are important for liquid-hydrogen and liquid-oxygen-fed bearings because of the low fluid kinematic viscosity values.

The ball bearing element's characteristics of fatigue life, stiffness, and friction torque were calculated as functions of axial and radial load for the applicable ranges of inner and outer race speeds using a computer program written by A. B. Jones (Ref. 5).

### Parametric Design Studies

To organize the large number of variables and interactions, nondimensional relations were combined into the design charts for liquid hydrogen and liquid oxygen hybrid bearings (Ref. 6). Studies were also made of the effects of manufacturing tolerance ranges and the use of surrogate fluids for test. It was found impractical to incorporate all hydrostatic bearing variables in universally applicable charts. However, a reasonable number of curves can be utilized to characterize bearings with the same recess configuration and similar Reynold's number. The use of nondimensional charts can effect a reduction in the computer time required to optimize the design for a particular application.

Examples of nondimensional parameters are the pressure ratio ( $\bar{P}_R$ ), nondimensional stiffness ( $\bar{K}$ ), and damping ( $\bar{B}$ ). The relation of  $\bar{K}$ ,  $\bar{B}$  to  $\bar{P}_R$  (Fig. 3) allows assessment of multiple dimensional variables with one chart. Other nondimensional parameters such as an L/D (journal length divided by diameter) and C/R (radial clearance divided by journal radius) can be used to assess bearing performance in response to a great many variables.

### Detail Designs

All four hybrid configurations shown in Fig. 2 were analyzed and detail designs produced. Table 2

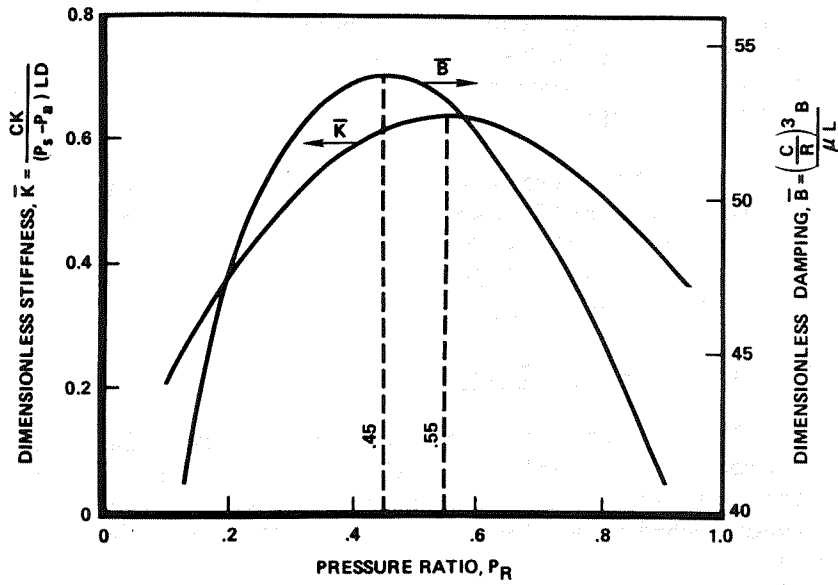


Fig. 3. Liquid Hydrogen Hydrostatic Bearing

Table 2. Hydrostatic Bearing Design Features

	HYDROSTATIC BEARING			
	EPS	EPL	IPL	IPS
DIAMETER, IN.	3.5	3.0	2.15	1.31
LENGTH, IN.	1.5	1.0	1.0	1.7
RADIAL CLEARANCE, IN.	0.00175	0.0015	0.0015	0.0009
ORIFICE DIAMETER, IN.	0.048	0.050	0.053	0.017
NO. OF RECESSES	12	6	6	12
RECESS AREA RATIO	0.08	0.1	0.1	0.08
NO. OF ROWS	2	1	1	2
RECESS WIDTH, IN.	0.183	0.449	0.322	0.274
RECESS LENGTH, IN.	0.300	0.350	0.350	0.340
SILL LENGTH, IN.	0.300	0.325	0.325	0.340

lists the major dimensional characteristics. In view of the existence of practical experience with EPS bearings and in the interest of gaining experience with new concepts, the EPL, IPL, and IPS configurations (Fig. 2B, C, and D) were fabricated as test bearings. The predicted major performance characteristics are listed in Table 3.

Table 3. Hydrostatic Bearings Performance

	HYDROSTATIC BEARING					
	EPS		EPL		IPL	IPS
	TURB.	INLET	TURB.	INLET		
<b>OPERATING CONDITION:</b>						
FLUID	LH <sub>2</sub>	LH <sub>2</sub>	LH <sub>2</sub>	LH <sub>2</sub>	LO <sub>2</sub>	LO <sub>2</sub>
SPEED, RPM	36,600	36,600	36,600	36,600	29,800	29,800
SUPPLY PRESSURE, PSIA	5,600	2,350	5,600	2,350	2,003	2,003
SUMP PRESSURE, PSIA	3,700	350	3,700	350	407	407
FLUID TEMPERATURE, R	90	90	90	90	196	196
<b>FLUID PROPERTIES:</b>						
VISCOSITY, LB-SEC/IN. <sup>2</sup> x 10 <sup>9</sup>	1.86	1.12	1.86	1.12	20.0	20.0
DENSITY, LB-SEC <sup>2</sup> /IN. <sup>4</sup> x 10 <sup>4</sup>	0.069	0.0473	0.069	0.0473	1.0	1.0
<b>PERFORMANCE:</b>						
FLOWRATE, LB/SEC	0.99	0.86	0.54	0.464	1.6	0.40
DIR. STIFF., LBF/IN. x 10 <sup>-6</sup>	3.49	3.55	1.59	1.69	1.09	2.27
CROSS-CPL. STIFF., LBF/IN. x 10 <sup>-5</sup>	2.87	2.30	1.00	0.81	2.4	10.2
DIR. DAMPING, LBF-SEC/IN.	150.3	121.0	52.4	42.5	152.4	655.3
PRESSURE RATIO	0.46	0.44	0.47	0.45	0.68	0.51
POWER LOSS, HP	2.71	1.92	1.02	0.71	2.21	0.66

In selecting the hydrostatic test bearing designs, priority was assigned to maximizing stiffness and damping with a satisfactory degree of stability. Optimization for some applications might require greater emphasis on achieving low friction torque or flowrate, resulting in alternate design details of clearance, recess configuration, and orifice diameter.

Initial sizing of the hydrostatic bearing may be dictated by turbopump design or selected from operating conditions by applying

$$\frac{W}{(P_s - P_a) L/D} \approx 0.25 \quad (1)$$

The radial clearance for the first design iteration can be assumed so that (Ref. 7):

$$C/R = 0.001 \quad (2)$$

The next step, selection of a recess configuration, is affected by several considerations. The recess volume should be limited to preserve stability, but the recess should be deep enough to achieve uniform pressure over the recess area. The number, length, and width of

the recesses should be chosen so that the recess to total bearing area ratio is less than 0.15 (an adaptation of MTI experience). The number of recesses should be four or more to achieve uniform directional load capacity, while the use of more than six is not generally necessary (Ref. 8). For EPS bearings, where the free-rotating member has considerable angular compliance, two rows of recesses are probably beneficial, which leads to more but smaller recesses.

After selecting the recess configuration, the compensating orifices are sized to achieve equal orifice and film flow resistances, producing near-maximum stiffness and damping as illustrated in Fig. 3. The computer program is then used to calculate the stiffness, damping, flow, and friction torque for comparison to design constraints.

If necessary, bearing geometric variations are repeated until the desired result is achieved. In general, increased stiffness, damping, and friction torque with decreased flow result from decreases in clearance or increases in length.

#### EPS Bearing

For maximum ball bearing life extension, the outer race cartridge speed should approach shaft speed as illustrated by Fig. 4. This condition requires that film friction be less than that of the ball bearings.

Such conditions are predicted for liquid hydrogen hybrid bearings, and have been confirmed experimentally (Ref. 1 and 2). However, use of liquid oxygen in a similar bearing will produce a relatively low speed ratio due to the higher fluid viscosity and density.

In the EPS bearing, the journal must be larger than the shaft to contain the ball bearing. Therefore, if the maximum speed is limited by the tensile strength of the cartridge to  $5 \times 10^6$  DN, the actual

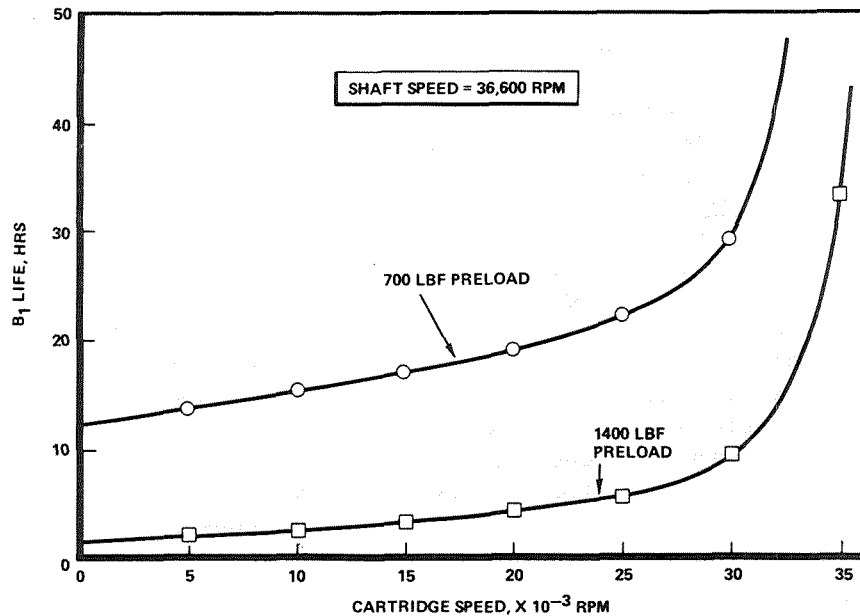


Fig. 4. 45-mm Ball Bearing Life  
(EPS Hybrid Bearing)

shaft-based DN limit will be in the range of  $3 \times 10^6$  DN, representing a significant extension to the unaided ball bearing speed limit of approximately  $2 \times 10^6$ .

In optimizing the EPS design, the relatively large centrifugal growth of journal diameter made it advantageous to reduce steady-state radial clearance to below the theoretical optimum so that a reduction could be made in clearance at start and low speed. The resulting greater stiffness throughout the speed range offset the disadvantage of higher friction. Because rotordynamic response may be sensitive to bearing stiffness and deadband, clearance tradeoffs should be part of the detail design of any EPS bearing. Conclusions drawn from the design studies for the EPS bearing are:

1. The EPS bearing can offer significant bearing life extension for high speed liquid

hydrogen applications. It should be considered for incorporation in the high pressure fuel turbopump.

2. The EPS bearing is not suitable for liquid oxygen use at high speeds.

### EPL Bearing

The EPL bearing offers significant increases over ball bearing load capacity and stiffness. By supporting a part of the radial load, ball bearing life is extended as shown in Fig. 5. This characteristic is desirable because life limitations for propellant-cooled bearings are chiefly caused by radial loading rather than axial preloads. A second significant advantage of the EPL bearing is that the hydrostatic film couples the journal directly to the housing thus making available all the stiffness and damping of the fluid film.

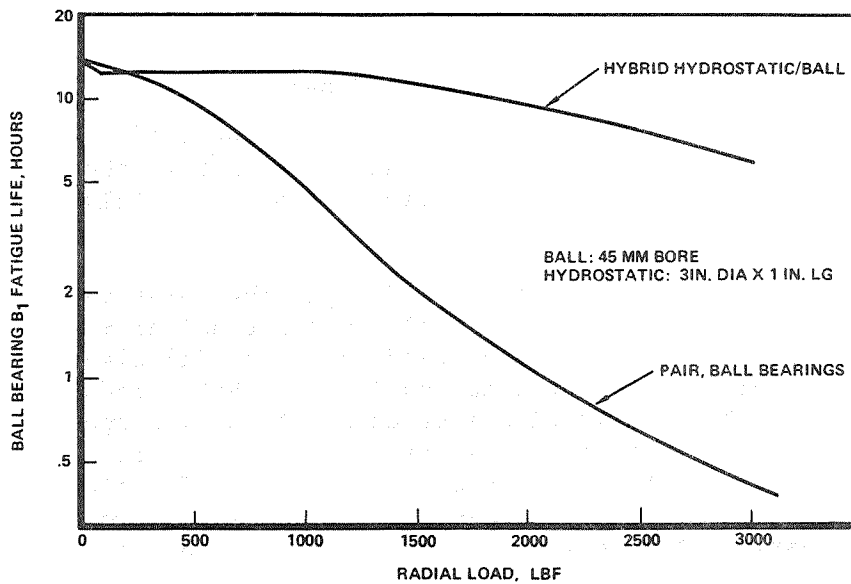


Fig. 5. Load Sharing Effect on 45-mm Ball Bearing Life (3- by 1-Inch Parallel Load Hybrid Bearing)

Rubbing during startup and shutdown can be reduced or avoided completely, a significant advantage for liquid oxygen bearings. Not only is the film clearance typically greater than the ball bearing OD clearance, but also the centrifugal growth of the journal can be advantageously used to increase the startup clearance. Conclusions concerning the EPL bearing were:

1. The EPL bearings' potential advantages warrant fabrication and test.
2. Although applicable to both liquid hydrogen and oxygen, the potential for avoidance or rubbing is of greatest advantage for liquid oxygen.
3. Due to direct coupling, the EPL bearing offers major benefits in terms of increased stiffness, damping, and load capacity.
4. Since ball bearing speed is not reduced, the speed and life increasing potential cannot approach that of the EPS bearing.

#### IPL Bearing

The IPL bearing offers the same increases in load capacity, stiffness, life, and avoidance of rubbing contact as noted for the EPL configuration. A potential disadvantage of unknown magnitude is the increased fluid tangential velocity that may result in increased cross-coupling effects. Conclusions relative to the IPL studies were similar to those for the EPL configuration. A test bearing was fabricated and tests are planned using liquid nitrogen and liquid oxygen.

#### IPS Bearing

Extension of life and speed can be obtained with liquid oxygen as well as liquid hydrogen when the IPS configuration (Fig. 2D) is employed. The reduced diameter of the hydrostatic bearing journal results in lower film friction, better speed ratio, and improved ball bearing life. For the IPS test bearing design, the film will theoretically assume 22,000 rpm

of the 30,000 rpm shaft speed, raising the ball bearing  $B_1$  life from 19 to 42 hours (Fig. 6).

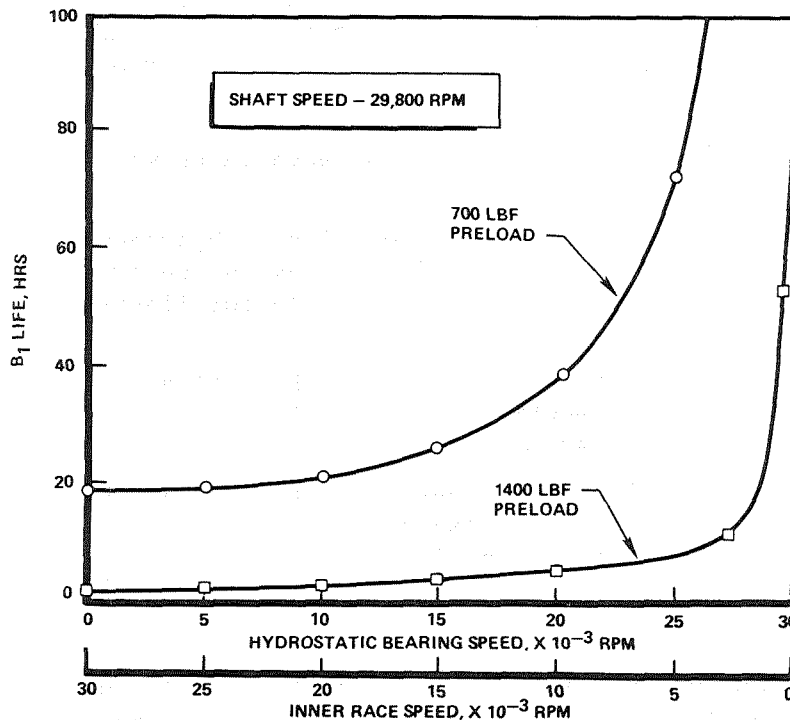


Fig. 6. 45-mm Ball Bearing Life vs Cartridge Speed (IPS Hybrid Bearing)

Additional advantages of the IPS bearing, when compared to the EPS configuration, include:

1. A speed limit of approximately  $5 \times 10^6$  DN is realizable, since only the shaft rotates at maximum speed.
2. Less kinetic energy dissipation will occur at touchdown during the shutdown transient because the cartridge is smaller.
3. Less centrifugal growth will occur, therefore less clearance change and sensitivity to speed will result.

4. The potential for internal feed exists in the high pressure oxidizer turbopump and the turbine end of the high pressure fuel turbopump.

As a consequence of internal feed, the working fluid's tangential velocity in the film will be higher, possibly increasing cross-coupling effects. Conclusions based on the IPS design studies are:

1. IPS bearing's potential advantages justify fabrication and test.
2. The IPS bearing is particularly advantageous in extending speed limits of ball bearings.
3. The IPS bearing is a viable candidate for the high pressure oxidizer turbopump and the high pressure fuel turbopump turbine bearing positions.

#### Damping Studies

To define the benefits of the damping available from hybrid bearings, studies were conducted to provide insight in three areas:

1. How much damping is desirable from a rotor-dynamic response aspect?
2. How much damping can be obtained from liquid hydrogen- and oxygen-fed hydrostatic bearings?
3. How can damping coefficient be confirmed empirically?

Using a rotordynamic model representation of SSME-type high pressure turbopumps, it was shown that the optimum magnitude of damping (that which attains the minimum response) increases with bearing stiffness. For the model used, Fig. 7 illustrates that added damping can increase response amplitudes below resonances, but may increase them at greater speeds. Optimum damping for the second resonant speed is greater than that for the first resonance. The conclusion

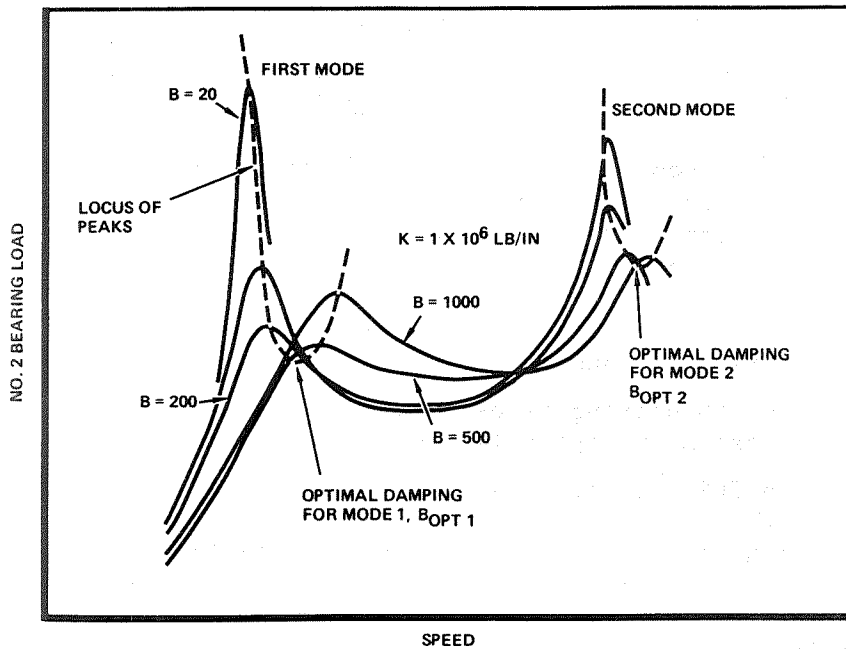


Fig. 7. Optimized Damping

drawn from the study is that optimization of damping requires a parametric study of bearing location, stiffness, and damping at the conceptual stage of rotor design.

#### Bearing Damping Potential

The magnitude of damping obtainable from liquid hydrogen and oxygen hydrostatic bearings was defined analytically in a parametric study of the effects of variations in bearing length, L/D, clearance, overall and film pressure ratios, recess geometry, orifice diameter, speed, eccentricity, and fluid properties. As shown in Table 4, the damping from a liquid hydrogen bearing responded most significantly to bearing size and clearance.

The magnitude of damping available from a similar sized liquid oxygen bearing was approximately four times that for liquid hydrogen, but the response to

Table 4. LH<sub>2</sub> Hydrostatic Bearing Damping Sensitivity

PARAMETER	SYMBOL	RANGE	DAMPING, Bxx, LBF-SEC/IN.		
			0	500	1000
L/D RATIO (D = 3.5")	L/D	.2 TO 1.0	[Bar chart showing sensitivity across the range]		
RADIAL CLEARANCE	C	.004" TO .003"	[Bar chart showing sensitivity across the range]		
SPEED (OVERALL EFFECT)	N	0 TO 40000 RPM	[Bar chart showing sensitivity across the range]		
L/D RATIO (LD = 5.25 IN <sup>2</sup> )	L/D	.2 TO 1.0	[Bar chart showing sensitivity across the range]		
PRESSURE DROP	(P <sub>s</sub> -P <sub>a</sub> )	1000 TO 5000 PSI	[Bar chart showing sensitivity across the range]		
SUPPLY/AMBIENT PRESSURE RATIO	P <sub>s</sub> /P <sub>a</sub>	1.5 TO 5.0	[Bar chart showing sensitivity across the range]		
PRESSURE RATIO	$\bar{P}_R$	.1 TO .7	[Bar chart showing sensitivity across the range]		
FLUID DENSITY	$\rho$	4 TO 9 (X 10 <sup>-6</sup> LB-S <sup>2</sup> /IN <sup>4</sup> )	[Bar chart showing sensitivity across the range]		
FLUID VISCOSITY	$\mu$	.5 TO 3.5 (X 10 <sup>-9</sup> LB-S/IN <sup>2</sup> )	[Bar chart showing sensitivity across the range]		
NUMBER OF RECESS	n	6 TO 20	[Bar chart showing sensitivity across the range]		
ECCENTRICITY RATIO	$\epsilon$	0 TO .9	[Bar chart showing sensitivity across the range]		
RECESS AREA RATIO	A <sub>r</sub>	.06 TO .15	[Bar chart showing sensitivity across the range]		
ORIFICE DIAMETER	d <sub>o</sub>	.032" TO .046"	[Bar chart showing sensitivity across the range]		
SPEED (SOLE EFFECT)	N	0 TO 40000 RPM	[Bar chart showing sensitivity across the range]		

geometric and operational variations followed a similar pattern (Table 5).

Table 5. LO<sub>2</sub> Hydrostatic Bearing Damping Sensitivity

PARAMETER	SYMBOL	RANGE	DAMPING, Bxx, LBF-SEC/IN.			
			0	1000	2000	3000
L/D RATIO (D = 3.5")	L/D	.2 TO 1.0	[Bar chart showing sensitivity across the range]			
RADIAL CLEARANCE	C	.0004" TO .003"	[Bar chart showing sensitivity across the range]			
L/D RATIO (LD = 5.25 IN <sup>2</sup> )	L/D	.2 TO 1.0	[Bar chart showing sensitivity across the range]			
SPEED (OVERALL EFFECT)	N	0 TO 30,000 RPM	[Bar chart showing sensitivity across the range]			
PRESSURE RATIO	$\bar{P}_R$	.1 TO .8	[Bar chart showing sensitivity across the range]			
PRESSURE DROP	(P <sub>s</sub> -P <sub>a</sub> )	200 TO 2,000 PSI	[Bar chart showing sensitivity across the range]			
PRESSURE RATIO	P <sub>s</sub> /P <sub>a</sub>	1.5 TO 6.0	[Bar chart showing sensitivity across the range]			
ECCENTRICITY RATIO	$\epsilon$	.0 TO .9	[Bar chart showing sensitivity across the range]			
FLUID DENSITY	$\rho$	.8 TO 1.2 (X 10 <sup>4</sup> LB-S <sup>2</sup> /IN <sup>2</sup> )	[Bar chart showing sensitivity across the range]			
SPEED (SOLE EFFECT)	N	0 TO 30,000 RPM	[Bar chart showing sensitivity across the range]			
FLUID VISCOSITY	$\mu$	.8 TO 3.0 (X 10 <sup>-8</sup> LB-S/IN <sup>2</sup> )	[Bar chart showing sensitivity across the range]			
NUMBER OF RECESSES	n	6 TO 20	[Bar chart showing sensitivity across the range]			
RECESS AREA RATIO	A <sub>r</sub>	.06 TO .15	[Bar chart showing sensitivity across the range]			
ORIFICE DIAMETER	d <sub>o</sub>	.025" TO .067"	[Bar chart showing sensitivity across the range]			

Damping Measurement

Empirical determinations of damping coefficients are planned to confirm analytic predictions. The

experimental method employs a journal eccentricity to produce a synchronous motion across the fluid film, which will be measured by proximity devices. Motions of the stator will be determined by proximity devices and accelerometers. Forces transmitted between the stator and the tester housing will be measured by strain gages in preloaded stiffening spokes. The dynamic force and motion data are to be recorded on magnetic tape for subsequent Fourier analysis to extract damping and stiffness coefficients.

#### Hardware Fabrication

The hydrostatic elements of the test bearings were constructed of Alloy 718 as were the mating parts of the tester to minimize relative thermal growths. Recesses in the EPL and IPL bearings were formed by EDM (Electric Discharge Machining). Recesses in the IPS journal are being produced by grinding.

Opposing materials in the EPL bearing for liquid hydrogen service are thin-dense chrome (bearing) vs bare Alloy 718 (journal). This combination was chosen to provide a wear-resistant surface to mate with the ball bearing outer diameter.

Both the IPL AND IPS bearings have thick silver-plated inner surface opposing chrome-plated journals following current practice in liquid oxygen turbopumps for potential rub locations.

#### Testing

The device shown in Fig. 8 was designed and built especially to test hydrostatic and hybrid bearings. Working fluid can be supplied through the test bearing housing for external feed, or, by the addition of a third shaft seal, through the shaft for internal feed. The rotor is turbine driven so that turbopump shaft speed and acceleration can be simulated. Fixed radial loads can be applied to the test bearing with a load cylinder acting on the bearing support flexure. Strain gages on the support beams are used to monitor

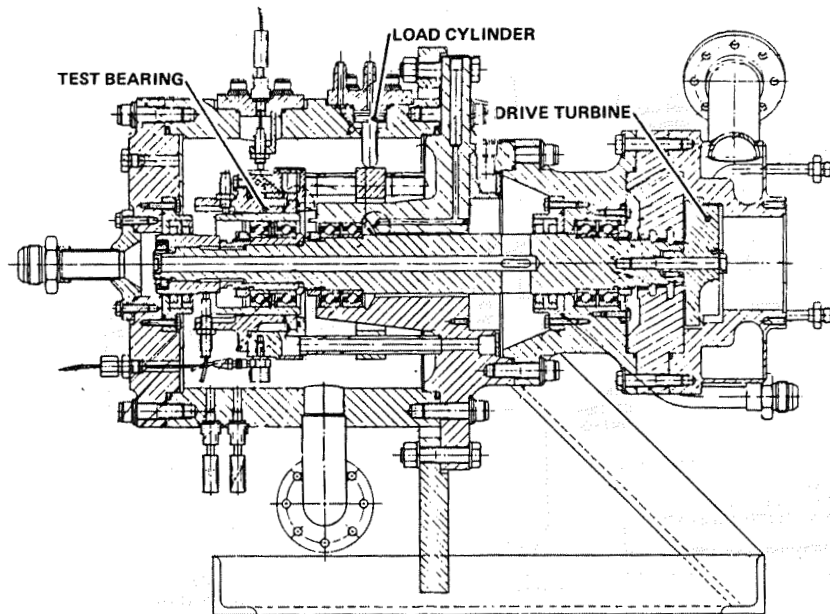


Fig. 8. Hybrid Bearing Tester

applied loads. Eddy current proximity devices are used to measure motions of the bearing and shaft, and also to measure speeds of the shaft and cartridge. For damping tests, a high bearing support stiffness is required to ensure measurable motion across the fluid film. In these tests, four strain-gaged spokes are radially pre-loaded against the test bearing housing to provide this additional stiffness. Strain gages and proximity probes were laboratory calibrated at ambient and liquid nitrogen temperatures.

The liquid hydrogen test facility, shown schematically in Fig. 9 provides liquid hydrogen for the test bearing supply from a 200-gallon tank. Gaseous hydrogen from a high-pressure source is used to pressurize the bearing supply, turbine drive, and load cylinder. Servocontrolled valves regulate test bearing supply and sump pressure, shaft speed, radial load, and when required, fluid inlet temperature. Timing of variations of each of these parameters can be controlled to six set points for a given test. Strip charts are used to monitor control function. Pressure, temperature

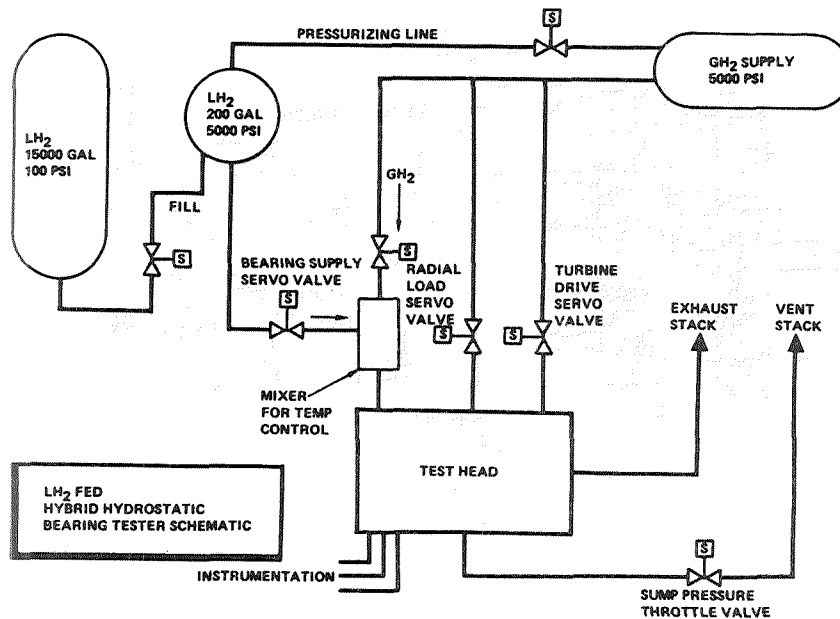


Fig. 9. Liquid Hydrogen Test Schematic

and speed data are recorded for later transcription to CRT plots. Digital data are tabulated for selected "time slices." Dynamic data from proximity devices and strain gages are recorded on FM tape for subsequent processing at the analog facility.

Redline cutoffs are used to terminate the test in the event of undesired test conditions of speed, pressures, temperatures, or accelerations.

Six bearing configurations were selected (Table 6) for testing with cryogenic working fluids (liquid hydrogen, nitrogen, or oxygen) under conditions of steady state and simulated turbopump transient start/shutdown. As previously described, eccentric journals will be used to extract dynamic coefficients of stiffness and damping.

### Test Results

In Test 012 (Table 7), flowrate was observed to decline as speed increased (Fig. 10) due largely to the

Table 6. Six Test Bearing Configurations To Be Evaluated

BUILD	DESCRIPTION	TESTS
1	EPL BEARING	STATIC AND PREPRESSURIZED ROTATING FLOW AND STIFFNESS TRANSIENT START AND SHUTDOWN
	LIQUID HYDROGEN FED ONE 45-MM BALL BEARING	
2	HYDROSTATIC ELEMENT OF BUILD 1 ECCENTRIC JOURNAL	DAMPING MEASUREMENT
3	INCREASED L/D HYDROSTATIC ELEMENT ECCENTRIC JOURNAL	DAMPING MEASUREMENT
4	IPL BEARING	STATIC AND PREPRESSURIZED ROTATING FLOW AND STIFFNESS TRANSIENT START AND SHUTDOWN
	LIQUID NITROGEN AND OXYGEN FED ONE 45-MM BALL BEARING	
5	HYDROSTATIC ELEMENT OF BUILD 4 ECCENTRIC JOURNALS	DAMPING MEASUREMENT
6	IPS BEARING	STATIC AND PREPRESSURIZED ROTATING FLOW AND STIFFNESS TRANSIENT START AND SHUTDOWN
	LIQUID NITROGEN AND OXYGEN FED PAIR OF 45-MM BALL BEARINGS	

Table 7. Test Result Summary

TEST NO.	TEST TYPE	SPEED, RPM	PRESSURES				TEMPERATURES		RADIAL LOAD, LB	STIFF 10 <sup>6</sup> LB/IN	FLUID INLET DENSITY	FLOW LB/SEC
			SUPPLY	SUMP	RECESS 1	RECESS 2	SUPPLY	SUMP				
012	LH <sub>2</sub> SPIN NO LOAD	8028	2357	352	1515	1511	104	87	0		3.56	0.37
		19564	2360	352	1585	1600	106	90	0		3.51	0.35
		32796	2358	353	1778	1799	112	97	0		3.38	0.31
019	LH <sub>2</sub> SPIN FIXED RADIAL LOAD	36676	2359	349	1859	1891	118	102	0		3.22	0.29
		38560	2328	346	1820	1894	91	82	0		3.58	0.32
		36065	2325	350	1816	1783	93	83	166	3.37	3.82	0.31
		36195	2324	349	1763	1831	93	83	0		3.82	0.32
		35624	2325	350	1859	1723	95	84	340	3.16	3.77	0.32
		36451	2326	350	1773	1845	95	84	0		3.78	0.32
022	LH <sub>2</sub> TRANSIENT	35824	2323	351	1891	1716	95	84	386	3.45	3.77	0.32
		0	100	~ 10	~ 40	~ 40	56	52	0		-	-
		39229	2106	284	1763	1726	84	81	300*		4.00	0.26
		36961	2252	349	1853	1788	90	82	800*		3.91	0.33
		27634	1704	270	1246	1168	94	76	470*		3.45	0.32
		37257	2264	352	1876	1798	94	84	800*		3.81	0.32
		15668	1611	258	1041	1039	96	78	~ 0		3.31	0.32

\*INTENDED LOAD, ACTUAL LOAD MAY BE LESS

clearance reduction as the journal grows centrifugally. Changes not attributable to journal growth are most probably due to increased hydrodynamic (Couette) flow in the film and increased flow resistance of the adjacent ball bearing as speed increases. When the ball bearing was removed for the damping tests, the resulting decrease in recess pressure and increase in flow was attributed to reduced restriction of flow to one

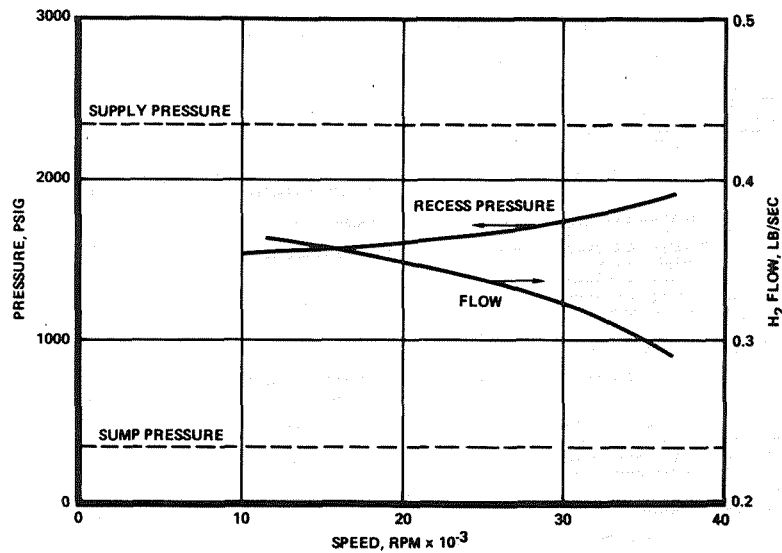


Fig. 10. Speed Effects - Test 012 EPL Bearing

side of the hydrostatic bearing. Based only on experimental results, correlation of the measured flow and recess pressures with analytic predictions suggests adjustments to the orifice discharge coefficient ( $C_D$ ) from the assumed 0.98 to 0.94. The lowered effective discharge coefficient may be the result of greater than normal losses due to fluid turbulence and sudden velocity changes at the orifice exit in the small recess volume. A corresponding adjustment is indicated for the land clearance entrance loss coefficient ( $K_e$ ) from the assumed 0.5 to 0.39. A possible reason for a lower-than-expected entrance loss is that the circumferential recess boundaries are tapered rather than being fully sharp due to the manufacturing process. Recess pressures showed an increase with speed (Fig. 10), corresponding to the flow decrease and also probably due chiefly to centrifugal journal growth. The decline in recess pressure that followed removal of the ball bearing was probably in response to lowered downstream flow resistance, even though that change applies to only one side of the bearing.

The calculated stiffness values from Test 019 are in the range of  $3 \times 10^6$  lb/in. for the composite total for the ball and hydrostatic bearing. Deducting the ball bearing calculated stiffness results in an apparent stiffness of  $2.7 \times 10^6$  lb/in. for the hydrostatic bearing, exceeding the predicted value by 70 percent. This result is comparable with those obtained by Hannum and Nielson (Ref. 3). Stiffness magnitude will be further assessed by comparison with the results of the damping tests and with repeated steady-state tests of the hydrostatic bearing alone.

Two transient tests based on the high pressure fuel turbopump start/shutdown profile were completed as programmed. Figure 11 illustrates the simultaneous ramps of speed, supply and sump pressures, and radial load as they would occur during launch, throttling, and shutdown in an SSME flight at the Challenger power levels. The simulated total run duration is compressed to avoid liquid hydrogen depletion prior to shutdown.

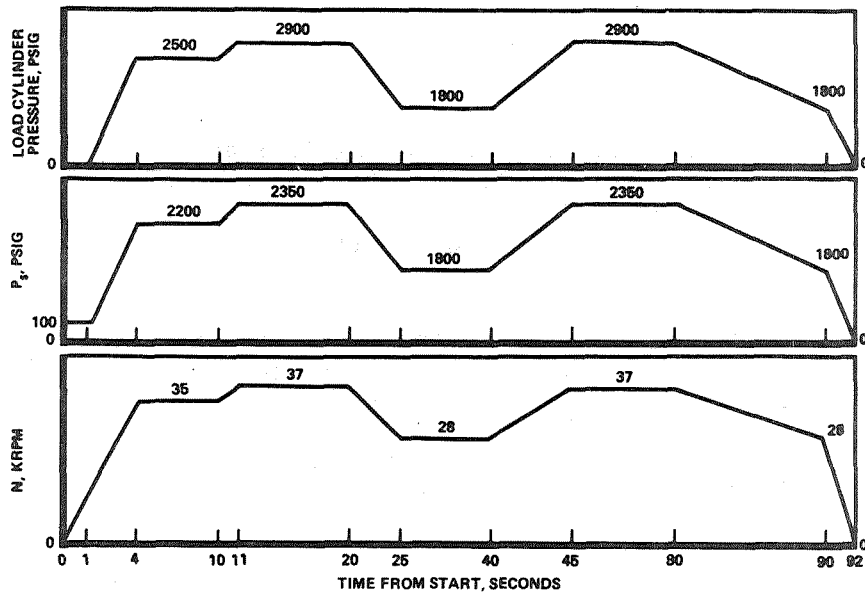


Fig. 11. HPFTP Start/Shutdown Transient  
(Challenger Profile)

Two damping tests were conducted incorporating an eccentric journal and stiffened bearing support. Three ramps were included at speeds from 10,000 to 14,000 rpm, 22,000 to 26,000 rpm, and 32,000 to 36,000 rpm. Data examination and analysis is currently underway.

### Looking Ahead

Analytic treatment and test results have shown that hybrid bearings have potential to improve turbopump bearing and rotordynamic performance, and that they are viable and practical machine elements. The current SSME Long Life Program will provide empirical and operational data concerning externally fed liquid hydrogen and oxygen hybrid bearings.

Two additional areas of study are recommended to support the incorporation of load sharing elements into current and future turbopump designs:

1. EPL (Externally Fed Parallel Load) hybrid bearings for liquid oxygen service
2. Load sharing seals for liquid oxygen - This concept is currently showing outstanding potential for extension of bearing life and improvement of rotor stability. An effort to quantify or confirm analytic seal coefficients for liquid oxygen operation would be extremely valuable.

These elements can be designed and fabricated for incorporation into the currently used test device for functional evaluation and correlation of analytic and test results.

### Nomenclature

- $A_o$  = orifice area, in.<sup>2</sup>  
 $A_r$  = recess area ratio =  $\bar{x} \bar{y}$   
 $B_{xx}$  = direct damping, lbf-sec/in.  
 $\bar{B}_{xx}$  = nondimensional damping  $(c/R)^3 B_{xx} / \mu L$

- $c$  = clearance, inches  
 $C_D$  = coefficient of discharge  
 $D$  = journal diameter, inches  
 $d_o$  = orifice diameter, inches  
 $g$  = gravitational constant = 386.4 in./sec<sup>2</sup>  
 $G_p$  = turbulent correction factor for viscosity  
 $K$  = stiffness, lbf/in.  
 $\bar{K}$  = nondimensional stiffness =  $cK/(P_s - P_a)$   
 $K_{xx}$  = direct stiffness, lbf/in.  
 $K_{xy}$  = cross-coupling stiffness, lbf/in.  
 $K_e$  = inertia coefficient  
 $L$  = bearing length, inches  
 $m$  = number of rows  
 $n$  = number of recesses  
 $N$  = rotational speed, rpm  
 $P_a$  = ambient pressure, psia  
 $P_r$  = recess pressure, psia  
 $P_s$  = supply pressure, psia  
 $\bar{P}_R$  = pressure ratio  
 $R$  = journal radius, inches (=  $D/2$ )  
 $\bar{R}_f$  = nondimensional film resistance =  $\left[ \frac{\rho g G_p c^3 \bar{P}_R}{\mu \left(\frac{L}{D}\right) \left(1 - \frac{\bar{Y}}{m}\right)} \right]^2 (P_s - P_a) R_f$   
 $R_o$  = orifice resistance, sec<sup>2</sup>/lb-in.<sup>2</sup>  
 $\bar{R}_o$  = nondimensional orifice resistance =  $\left[ \frac{\rho g G_p c^3 \bar{P}_R}{\mu \left(\frac{L}{D}\right) \left(1 - \frac{\bar{Y}}{m}\right)} \right]^2 (P_s - P_a) R_o$

W = bearing load, lbf

$\epsilon$  = eccentricity ratio

$$\Lambda_r = \text{orifice restrictor parameter} = \frac{\rho(P_s - P_a) c^6 R}{\mu(A_o C_D)^2}$$

### References

1. Wolf, J. E., Mark 25 Pump Hybrid Hydrostatic Bearing Test at Nuclear Rocket Development Station, Rockwell International/Rocketdyne Division, Canoga Park, CA, Report R-9117, Contract SNSN-65, 20 November 1972.
2. Hannum, N. P. and C. E. Nielson, "The Performance and Application of High Speed Long Life LH<sub>2</sub> Bearings for Reusable Rocket Engine Turbomachinery," NASA TM-83417, AIAA 83-1389, June 1983.
3. Reddecliff, J. J. and J. M. Vohr, "Hydrostatic Bearings for Cryogenic Rocket Engine Turbopumps," J. of Lubrication Technology, July 1969.
4. Artiles, A., J. Wallowitz, and W. Shapiro, "Analysis of Hybrid, Fluid Film Journal Bearings With Turbulence and Inertia Effects. Advances in Computer-Aided Bearing Design," Proceedings of ASME-ASLE Lubrication Conference, American Society of Lubrication Engineers, New York, October 1982.
5. Jones, A. B., Rolling-Element Bearing Analysis Program, 1978.
6. Lee, F. C., Parametric Study of Hybrid Bearings, Rockwell International IL TPME 3172-6642, 23 November 1982.
7. Vohr, J. H., Journal Bearing Section, RPI-MTI Gas Bearing Design Course, 1967.
8. Aston, R. L. and J. P. O'Donoghue, "The Effect of the Number of Recesses on the Performance of Externally Pressurized Multi-Recess Journal Bearings," Tribology, May 1971.